JOURNAL OF OPTOELECTRONICS AND ADVANCED MATERIALS Vol. 25, No. 5-6, May – June 2023, p. 294 - 301

Polarization mechanisms of $TlSbS_2$ thin films

SAHIN YAKUT, DENIZ DEGER, DENIZ BOZOGLU, KEMAL ULUTAS*
Istanbul University, Science Faculty, Physics Department, Vezneciler/Fatih/Istanbul, 34134, Turkey

$TlSbS_2$ is a material having good photovoltaic and thermoelectric properties in bulk form. Electrical characteristics are important to analyze such properties as photovoltaic and thermoelectric. Improvements in industrial and technological applications required materials having low size. Thus, it is important to analyze this material in nano-size dimensions. For this reason, $TlSbS_2$ was investigated in thin film form. To make the detailed characterization of dielectric properties enabled, the dielectric investigation of $TlSbS_2$ thin films was operated depending on frequency, temperature, and film thickness. In this study, TlSbS2 thin films are produced by the deposition of $TlSbS_2$ bulk samples by thermal evaporation on glass substrates. The thicknesses of the films are between 49 and 619 nm. The dielectric properties and ac conductivity of the $TlSbS_2$ thin films at a temperature range 293-373 K are measured over a frequency range between 20 Hz and 1kHz. The dielectric constant increases with increasing thickness starting from almost 10 to almost 30. Two polarization mechanisms are observed. One of them can be related to the interfacial polarization of partially free charge carriers including atom groups constructed from combinations of Tl, Sb, and S or individual atoms of Tl, Sb, and S. The polarization of bonds between Tl-S and Sb-S inside local crystal states can be attributed to orientational (dipolar) polarization. Activation energies of the polarization mechanisms are determined. In addition to dielectric spectroscopy measurements, XRD analysis results show that the $TlSbS_2$ bulk samples (raw samples used for the deposition of thin films) are in crystalline form. However, $TlSbS_2$ thin films deposited from $TlSbS_2$ bulk samples by thermal evaporation are found to be amorphous. The relationship between the structure of the material and its dielectric properties is studied.

(Received May 23, 2022; accepted June 9, 2023)

Keywords: $TlSbS_2$ compounds, Thin films, dielectric properties, AC conductivity, Thickness dependence

1. Introduction

$TlVVI_2$ ternary compounds (Here V and VI represent 5A and 6A group elements, respectively) are attractive materials because of their anisotropy and some physical properties based on easily detectable layered structures. Based on directions on layers physical properties can change as a result of the anisotropic characteristic. This characteristic property causes variation in physical properties for bulk Thallium antimony disulfide ($TlSbS_2$). $TlSbS_2$ is one member of this compound family. $TlSbS_2$ has a triclinic structure [1–3]. $TlSbS_2$ has an optical bandgap of around 1,69 eV with a strong interest area for the visible-infrared region as optical absorber material [4,5]. These compounds have good photovoltaic (optical band gap is 1,42 eV) [6] and thermoelectric properties (lattice thermal conductivity; ZT number is 1,10 W/mK) [7] and are attractive for 3D topological applications [8,9]. That is, under hydrostatic pressure $TlSbS_2$ turns from semiconductor to semimetal due to phase transitions biaxial and uniaxial strain [9]. This compound has a melting point between 653-757 K [8]. There are remarkable studies on $TlSbS_2$ in the past. In one of these studies, the ultraviolet reflectivity of $TlSbS_2$ was investigated [10]. In another study, optical phonons and chemical bonding of $TlSbS_2$, $TlSbSe_2$, and Tl_3SbS_3 crystals were compared [3]. In a study in 2002, $TlSbS_2$ and $TlBiS_2$ were deposited as multilayered structures and investigated [4]. Thermodynamic properties of $TlSbS_2$ were investigated in 2016 [8]. In 2017, $TlSbS_2$ was detected as a hard radiation detector material [1]. A topological investigation of $TlSbS_2$ was operated in another study The drift mobility of electrons in $TlSbS_2$ was investigated by the study in 1986 [5]. Almost for all studies in literature, $TlSbS_2$ was investigated as a bulk or crystalline structure. Only in the study, investigating the physical properties of $TlSbS_2$ and $TlBiS_2$ multilayered structure has dimensions as the thin film [4]. But the only study work on the other physical properties of $TlSbS_2$ thin films was presented by our group in 2013 [2]. In this study, we worked on the structure and dielectric properties of bulk $TlSbS_2$ and the $TlSbS_2$ thin fila m with a thickness of 400 nm. The bulk $TlSbS_2$ was supplied by the acknowledged scientist of this study, Prof. Mehmet Ozer, who has opportunities to grow bulk binary and ternary compounds samples. $TlSbS_2$ thin film was deposited from bulk $TlSbS_2$ by thermal evaporation technique on glass substrates. Detailed information on the production phase is given in the experimental part. There is a comparison in this study. It was observed that the bulk form of $TlSbS_2$ has a crystalline structure while the thin film form of $TlSbS_2$ has an amorphous structure.

This study is aimed to evaluate the dielectric properties of $TlSbS_2$ thin films in a wide thickness range changing between 49-619 nm. The possible polarization mechanisms will be defined by using dielectric spectroscopy data. We will give information about the critical thickness which is a border between the thin film and bulk properties. It is expected to observe an exponential increase with increasing thickness until a

certain thickness which is called the border between dielectrically thin film characteristics and bulk characteristics. Over this border thickness, we hope to see thickness-independent dielectric constant behavior. Also, possible polarization mechanisms in the structure will be evaluated in frequencies between 20 Hz and 1kHz and 293-373 K temperature range. $TlSbS_2$ is a material having high photosensitivity and optical transparency. The nature of the polarization mechanism is important for defining the nature of photosensitivity and optical transparency. The definition of polarization mechanisms, which is one of the purposes of this study, can give information about the quality of these materials for the application areas such as photo-receiver, photo transducers, detectors of pulsed laser radiation, thermoelectric devices, and solar cell [2,5,10-13]. By this investigation, it will be enabled to have information on the physical features of $TlSbS_2$ thin films to adapt these thin-film materials to application areas in nanosize.

2. Experimental

To produce $TlSbS_2$ thin films, $TlSbS_2$ bulk granules were supplied by Prof. Mehmet Ozer who prepared the bulk $TlSbS_2$ samples by the Bridgman-Stockbarger technique [14-17]. The thermal evaporation method was operated on granules for thin-film production. During the deposition, the granules were turned into a vapor state by thermal effect. Deposition of thin films was progressed on microscope slides (76 mm x 24 mm x 1 mm) under vacuum conditions of 10^{-5} Torr (molybdenum boat with the thickness and width of 0.1 mm and 5 mm, respectively). Edwards (type 6E4) model thin film deposition system was used. The process temperature for thermal deposition was between 773K (≈500°C) and 823K ((≈550°C) [1]. The substrate was placed 10 cm away from the source while depositing. The required amount of mixture including powder and granules of $TlSbS_2$ was placed in the boat for deposition. The amount was changing between 50 and 400 mg depending on the planned film thickness. $TlSbS_2$ thin films were deposited between Au (gold) electrodes to obtain capacitive samples which are suitable for dielectric spectroscopy measurements with suitable masks. The thicknesses of thin films were determined by Tolansky's interferometric method. Samples with thicknesses of 49, 74, 282, 352, 424, 532, and 619 nm were prepared. The contact type of Au/TlSbS2/Au samples is detected as ohmic. An annealing process was operated at a 10^{-4} Torr vacuum and 433 K temperature for 10 minutes for all samples. In this way, reproducible measurements were obtained. The electrical resistance of the thin film samples was between 200 and 500 kΩ. Dielectric spectroscopy measurements were operated by an impedance analyzer (Hewlett Packard 4192A). The working potential difference was 1-volt rms. The frequency and temperature range were 20 Hz -1 kHz and 293-373 K, respectively. Frequency and temperature-dependent electrical capacitance (C) and dielectric dissipation (tanδ) were obtained from measurements. Then other dielectric parameters such as dielectric constant (ε'), and AC conductivity (σ_{AC}) were derived by suitable equations. In addition to dielectric spectroscopy measurements, X-ray diffraction measurement was operated to see the crystallographic situation. Rigaku DMAX 2200 model device was used for XRD measurements. XRD measurements were operated by an X-ray diffractometer using CuKα radiation between 2θ angle range from 0° to 90°.

3. Results

3.1. Crystallographic characterization of $TlSbS_2$ thin films

The XRD graphs in Fig. 1 are the graphs shared in our previous study on the same sample [2]. In Fig.1, XRD pattern for bulk (granule) $TlSbS_2$.

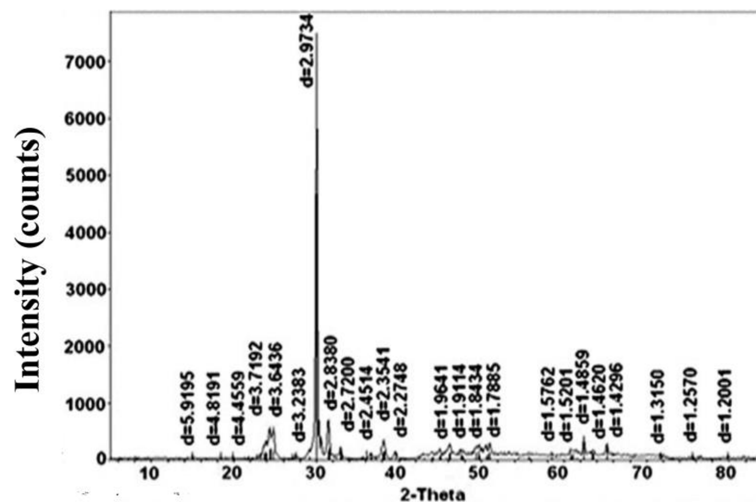

Fig. 1. XRD patterns for bulk $TlSbS_2$

It is observed that $TlSbS_2$ has a crystalline structure with a characteristic peak at a 2Θ angle of 30° as known from JCPDS cards 37-1342 and 29-1331. Both cards show that the crystalline structure is triclinic. These parameters are *a* =6.123 Å_101.34°, *b* = 6.293 Å _98.39°, and *c* = 11.838 Å_103.21°. Also, detailed information on structural and other physical properties can be followed in the literature [18].

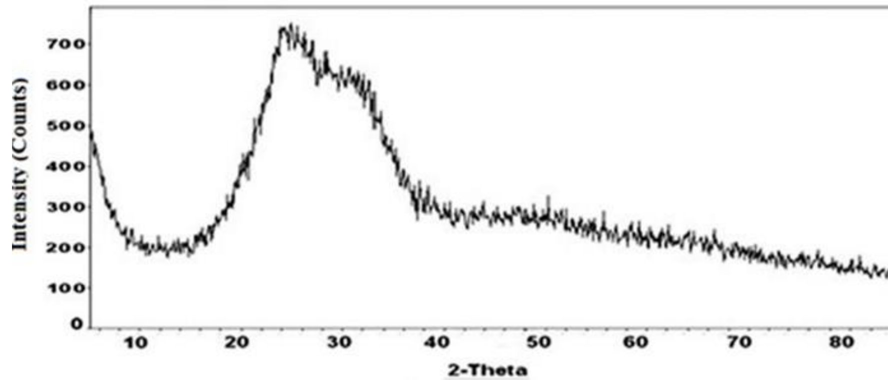

Fig. 2. XRD patterns for $TlSbS_2$ thin film samples

XRD pattern for $TlSbS_2$ thin films is presented in Fig. 2. It can be detected that the structures of thin films are amorphous [19,20]. Here, it can be concluded that during the agglomeration of atoms as a result of thermal evaporation, atoms could not find sufficient time and conditions to succeed in crystallization and the random placing of atoms occurred. Nevertheless, around 2Θ angle of 30°, there is a behavior indicating the presence of the groups involving the components of the $TlSbS_2$ lattice in Fig.2.

3.2. Frequency, temperature, and thickness dependence of dielectric constant (ε′)

It can be observed that the dielectric constant decreases with increasing frequency and in cases with increasing temperature as shown in Fig.3.

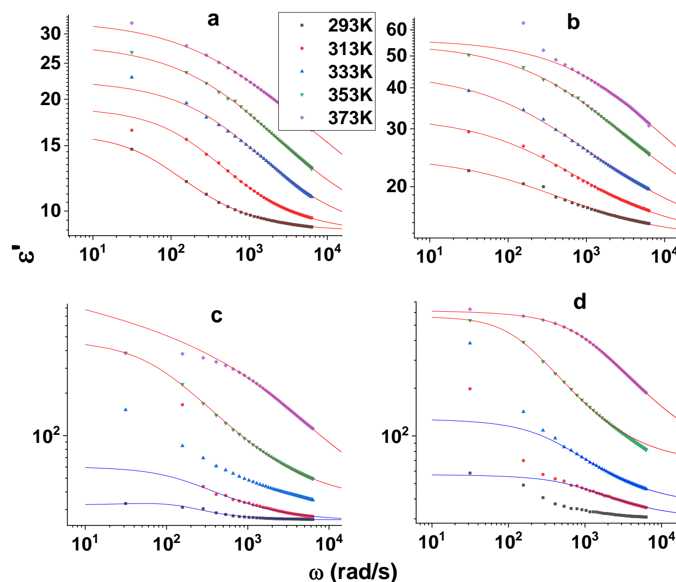

Fig. 3. Frequency and temperature-dependent dielectric constant ε′ for samples with a) 49 nm, b) 74 nm, c) 352 nm, d) 619 nm thickness (color online)

One of the electrical parameters to distinguish materials from each other is the dielectric constant. But for thin films, the dimension directly affects the dielectric constant because of the possible change of the atomic composition while the film structure is constructed at the time of agglomeration [21]. When frequency and temperature dependence of the dielectric constant is investigated for all samples, it is observed that the dielectric constant increases with increasing thin film thickness. Some representative figures are given in Fig. 3.

Also, it is observed that the dielectric constant increases directly proportional to thin-film thickness for all samples. For thin films with thicknesses over 74 nm, it is possible to observe two polarization mechanisms as shown in Fig. 3 (c) and Fig. 3 (d). The polarization mechanisms are determined by Cole-Cole fits which can be described in Equation 1.

$$\frac{\varepsilon^*(\omega)-\varepsilon_\infty}{\varepsilon_S-\varepsilon_\infty} = \frac{1}{1+(i\omega\tau_{CC})^\beta} \quad (1)$$

where ε^* is the complex dielectric function, ε_∞ is the dielectric constant at infinitely high frequencies, ε_s is the dielectric constant at a state without frequency, ω is the angular frequency, τ_{CC} is relaxation time and β is the broadening coefficient which has values between 0 and 1 [22-24]. In Fig.3c and Fig.3d, the blue Cole-Cole fit lines represent the polarization mechanism observed at low temperatures and the red fit lines represent the polarization mechanism that is dominant at high temperatures. There are four possible polarization mechanisms for amorphous materials. These mechanisms are interfacial or space-charge polarization, dipolar, ionic, and electronic polarization mechanisms [25,26]. It is known from the XRD results in section 3.1 that the $TlSbS_2$ thin film structure is amorphous while the $TlSbS_2$ bulk material has a crystalline structure. Increasing thickness may cause to decrease in void density [20]. Thus, there may be more interfacial regions between grains structure for some possible partially free-charge carriers. This result can be related to increasing the dielectric constant, especially at low frequencies with increasing thickness, and the appearance of a second polarization mechanism in the focused frequency region [25]. Both interfacial and dipolar polarization mechanisms can be observed at frequency regions between 0-1kHz. Here the temperature can be used to classify them. The mechanism represented by blue fit lines can be attributed to dipolar polarization of lattice or crystalline regions distributed to the amorphous structure while the red fit line can be attributed to interfacial polarization which appears with increasing film thickness as shown in Fig.3. The thickness dependence of the dielectric constant is shown in Fig.4a and Fig.4b. It is observed that the dielectric constant increases with increasing thickness starting from almost 10 to almost 30 as detected in Fig.4a.

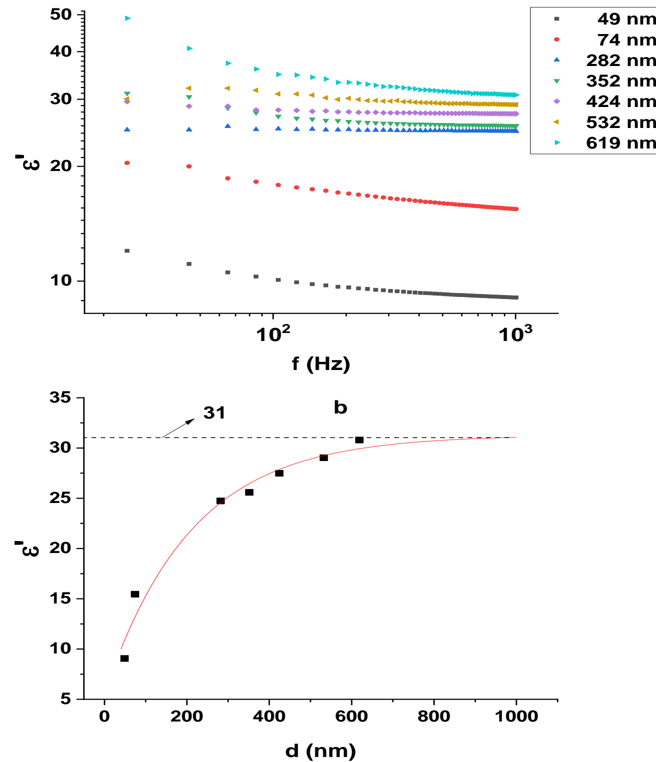

Fig. 4. a) Frequency dependence of dielectric constant at room temperature (293K) for all thicknesses, b) Thickness dependence of dielectric constant at 293K and 1kHz (color online)

It is reported that the change in void density is the reason for the change of dielectric constant depending on thickness [20]. If the bulk behavior limit is investigated for the dielectric constant as represented in Fig. 4b, it is observed that the dielectric constant increases exponentially with thickness until the dielectric constant value 31. The value, 31, is reached at a thickness of 950 nm. Following this thickness, the dielectric constant stays constant at 31. The thickness of 950 nm can be accepted as the critical thickness at which the sample behaves like a bulk sample in electrical meaning. Starting with the thickness of 950 nm the dielectric constant of $TlSbS_2$ thin

film is not affected by the change of film thickness since the influence of void density in the structure of thin film drops to a non-effective level.

3.3. Frequency, temperature, and thickness dependence of dielectric dissipation (tanδ)

Dielectric dissipation is the ratio between the imaginary or loss part and the real part of the dielectric function, impedance, and electric modulus, that is, functions belonging to electrical parameters as described in Equation 2.

$$tan\delta = \frac{\varepsilon''}{\varepsilon'} \quad (2)$$

In Fig. 5 representative figures of the frequency and temperature dependence of tanδ can be shown for some thicknesses.

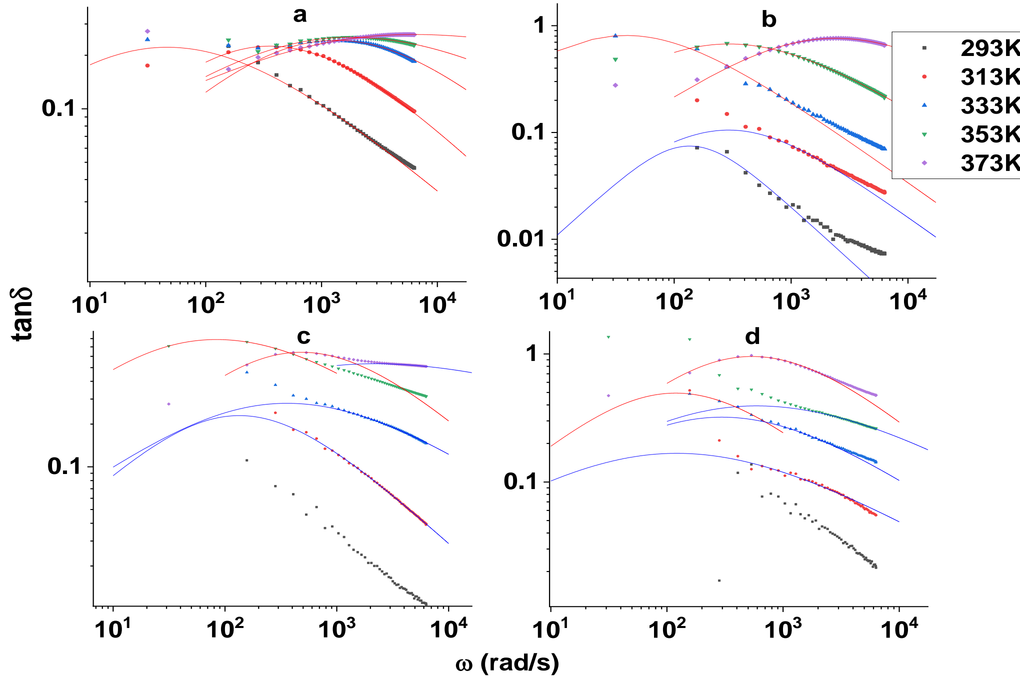

Fig. 5. Frequency and temperature dependence of dielectric dissipation (tanδ) for samples with a thickness of a) 49 nm, b) 282 nm, c) 424 nm, d) 532 nm (color online)

The presence of two polarization mechanisms can be observed at the frequency and temperature-dependent behavior of tanδ as shown in Fig.5b,c,d. As mentioned in the previous part based on the behavior of the dielectric constant, the blue fit lines derived for tanδ from the Cole-Cole equation represent the polarization mechanism detected at low temperatures and red lines represent the polarization mechanism detected at high temperatures. It is known from our previous study, the structure has an amorphous character as the thin film [2]. Although, the thin films are called $TlSbS_2$, because of the nature of the thermal evaporation technique the produced vapor does not include $TlSbS_2$ crystal. The produced vapor can be defined as a vapor including some $TlSbS_2$ groups but a lot of groups that are derivative of $TlSbS_2$ constructed by Tl, Sb, and S individually and their combinations [27-29]. By considering this, the polarization mechanism observed at high temperatures can be related to the interfacial polarization of partially free charge carriers including atom groups constructed from combinations of Tl, Sb, and S or individual atoms of Tl, Sb, and S [30]. The polarization mechanism which is observed at low temperatures and higher frequencies can be attributed to the orientational (dipolar) polarization of bonds between Tl-S and Sb-S inside local crystal states [30,31]. Red fit lines can be called interfacial polarization as mentioned in the previous section.

3.4. Frequency, temperature, and thickness dependent that AC conductivity (σ_{AC})

In Fig. 6 some representative figures can be shown for the frequency and temperature dependence of AC conductivity. AC conductivity behavior obeys Jonscher's Universal equation described in Equation 3.

$$\sigma_T = \sigma_{AC}(\omega) + \sigma_{DC} = \sigma_{DC} + A\omega^s \quad (3)$$

where σ_T is total conductivity, $\sigma_{AC}(\omega)$ is AC conductivity, σ_{DC} is Dc-conductivity or it is called the frequency-independent part of total conductivity, A is temperature-independent constant and s is frequency exponential [20].

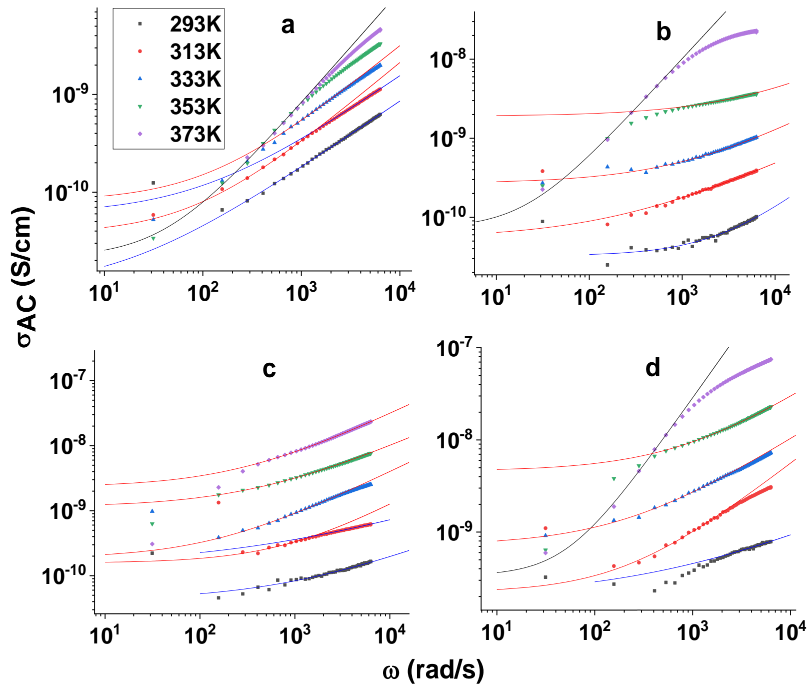

Fig. 6. Frequency and temperature dependence of AC conductivity (σ_{AC}) for thin films with thicknesses of a) 74 nm, b)282 nm, c) 424 nm, and d)532 nm (color online)

Blue fit lines are attributed to the polarization detected at low temperatures and the red fit lines are attributed to the polarization at high temperatures. In addition to the polarization mechanisms which are familiar from previous sections, there is a third polarization mechanism which is observed at 373 K and the low-frequency side. This mechanism is represented by black fit lines. Generally, it can be detected that the AC conductivity is greater for the mechanism shown with red fit lines. Especially, at high temperatures the frequency-independent part of AC conductivity has values around 10^{-8} S/cm. This result supports the situation of the mechanism with red fit lines being a bigger-sized polarization mechanism (interfacial) than the mechanism with blue fit lines [32,33]. The mechanism demonstrated by blue fit lines has frequency-independent conductivity values around 10^{-10} S/cm. Although a third polarization mechanism is observed at AC conductivity graphs at 373 K, as a general result two polarization mechanisms are detected in whole samples. To analyze the effect of thickness on polarization and the origin of polarization, the activation energies are detected as shown in Fig.7. Fit lines are generated by Equation 4.

$$ln\sigma_{AC} = ln\sigma_0 - \frac{\Delta E}{k_B T} \quad (4)$$

where ΔE is the activation energy, which is the minimum required thermal energy to cause polarization of a charged entity in structure, k_B is Boltzmann constant, which has a value of $8{,}617\text{x}10^{-5}$ eV/K and T is the temperature in Kelvin [2].

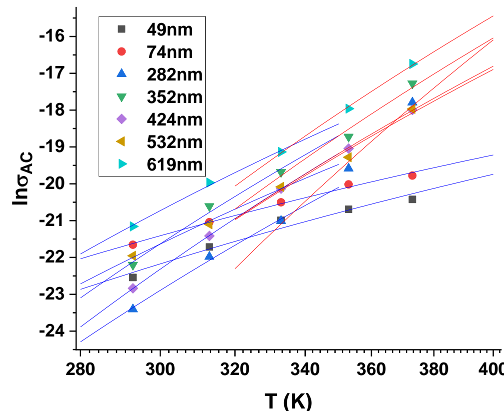

Fig. 7. The activation energies obtained from the temperature dependence of AC conductivity at 500Hz (color online)

Blue fit lines are attributed to the polarization detected at low temperatures and the red fit lines represent the polarization at high temperatures in comparison to the former mechanism. When the blue fit lines are investigated, it is observed that the activation energy changes between 0,22 and 0,53 eV. Besides, it is remarkable that the activation energies for thicknesses of 49 and 74 nm are the least two values 0,25 and 0,22 eV, respectively. Also, for 49 and 74 nm samples there is only one activation behavior. The red fit lines have activation energies changing between 0,56 and 0,85 eV. When the activation energies of 352, and 424 nm thin films are considered, these samples have the least two values as 0,57 and 0,56 eV. AC conductivity results support the results obtained from tanδ behavior. But the activation energy values are close to each other for two different polarization regions. The two-fold ratio between the activation energies of blue and red fit lines supports the evaluations in previous regions to analyze the nature of the mechanisms detected in the frequency and temperature regions [34].

4. Conclusion

The dielectric properties of so-called $TlSbS_2$ thin films, which are constructed by variation of molecules and cells involving Tl, Sb, and, S, deposited in different thicknesses changing between 49 and 619 nm by thermal evaporation of $TlSbS_2$ bulk granules that were grown by the Stockbarger Bridgman technique were investigated. XRD analysis shows that the thin film samples have an amorphous structure while $TlGaS_2$ granules, which are the source of thin film deposition, have a crystalline structure. The dielectric constant, dielectric loss and ac conductivity of the samples have been calculated by measuring capacitance and dielectric loss factor in the frequency range 20 Hz -1 KHz and temperature range 273-393 K. In the given intervals, it is observed that both dielectric constant and dielectric loss decrease with frequency, but increase with temperature._it is observed that the dielectric constant increases with increasing thin film thickness until a thickness-independent value, 31. The thickness at which the thickness-independent value is reached is 950 nm. This thickness can be accepted as the critical thickness at which the sample starts to behave like a bulk sample in electrical meaning. The presence of two polarization mechanisms was observed at the frequency and temperature-dependent behavior of tanδ and C from Cole-Cole fits. One of them which is observed at high temperatures can be related to the interfacial polarization of partially free charge carriers including atom groups constructed from combinations of Tl, Sb, and S or individual atoms of Tl, Sb, and S. The other which is observed at low temperatures high frequencies can be attributed to the orientational (dipolar) polarization of bonds between Tl-S and Sb-S inside local crystal states. A third polarization mechanism was observed at 373 K and low-frequency side from ac conductivity behavior**.** It was detected that activation energies calculated for the mechanism represented by red fit lines have average values around 0,6 eV. This mechanism was attributed to interfacial polarization due to partially free charge carriers. The mechanism represented by blue fit lines has activation energies around 0,3 eV. This mechanism was attributed to dipolar polarization. The two times difference supports the difference of nature between the two mechanisms observed dominantly among the samples investigated. $TlSbS_2$ thin films have smaller dielectric constant than $TlSbS_2$ bulk samples because of their amorphous characteristics. But still, the dielectric constant has values around 31 at the thin film-bulk border. These values can make these thin films effective thermoelectric materials for micro-thermoelectric applications because of the thickness size of these films.

Acknowledgments

We would like to thank Professor Mehmet Ozer who grew the samples. This work was supported by the projects funded by the Department of Scientific Research Projects of Istanbul University (I.U. BAP) [grant numbers 3569, 37896, 6481, 1785, 45032, 7366, and 30048].

References

[1] W. Lin, H. Chen, J. He, C. C. Stoumpos, Z. Liu, S. Das, J. Kim, K. M. McCall, B. W. Wessels, M. G. Kanatzidis, ACS Photonics **4**(11), 2891 (2017)
[2] M. Parto, D. Deger, K. Ulutas, S. Yakut, Appl. Phys. A Mater. Sci. Process. **112**(4), 911 (2013)
[3] N. N. Syrbu, V. T. Krasovsky, I. N. Grincheshen, Cryst. Res. Technol. **28**(3), 371 (1993).
[4] V. Estrella, M. T. S. Nair, P. K. Nair, Semicond. Sci. Technol. **17**(11), 1198 (2002).
[5] K. Čermák, P. Lošťák, Czechoslov. J. Phys. **36**(6), 709 (1986).
[6] Q. A. Adeniji, K. Odunaike, D. A. Leshi, A. J. Talabi, A. T. Adeleke, A. O. Abe, R. E. Momoh, F. B. Musah, Jordan Journal of Physics **14**(3), 249 (2021)
[7] V. A. Bazakutsa, M. P. Vasilieva, V. N. Ustimenko, L. M. Mokhir, J. Eng. Phys. **37** (4), 1191 (1979)
[8] Y. I. Jafarov, S. A. Ismayilova, Z. S. Aliev, S. Z. Imamaliyeva, Y. A. Yusibov, M. B. Babanly, Calphad Comput. Coupling Phase Diagrams Thermochem. **55**, 231 (2016)
[9] Q. Zhang, Y. Cheng, U. Schwingenschlögl, Sci. Rep. **5**, 8379 (2015).
[10] M. Merkel, C. Klient, H. Neumann, J. Horak, Cryst. Res. Technol. **28**, 629 (1993).
[11] X. X. Huang, X. G. Tang, X. M. Xiong, Y. P. Jiang, Q. X. Liu, T. F. Zhang, J. Mater. Sci. Mater. Electron. **26**(5), 3174 (2015)
[12] Z. G. Özdemir, Ö. A. Çataltepe, Ü. Onbaşlı, Int. J. Mod. Phys. B **29**, 1550205 (2015).
[13] T. Han, M. Josh, H. Liu, Journal of Petroleum

Science and Engineering **172**, 436 (2019).
[14] H. F. Mohamed, X. Changtai, S. Qinglin, C. Huiyuan, P. Mingyan, Q. Hongji, J. Semicond. **40** (1), 011801 (2019)
[15] https://wiki.aalto.fi/display/SSC/Bridgman+and+Stockbarger+methods
[16] X. Wang, N. Ma, J. Thermophys. Heat Transf. **20**(2), 313 (2006).
[17] A. F. May, J. Yan, M. A. McGuire, J. Appl. Phys. **128**(5), 051101(2020)
[18] http://webmineral.com/data/Weissbergite.shtml#.YlUWkHhBzIW
[19] K. Ulutas, D. Deger, S. Yakut, J. Phys. Conf. Ser. **417**(1), 012040(2013).
[20] D. Deger, K. Ulutas, S. Yakut, H. Kara, Mater. Sci. Semicond. Process. **38**, 1 (2015)
[21] P. Deng, Q. Jiao, H. Ren, J. Energ. Mater. **38**(3), 253 (2019).
[22] F. Kremer, A. Schönhals, Broadband Dielectric Spectroscopy. Broadband Dielectric. Spectrosc. Springer, Berlin Heidelberg, 2003.
[23] O. Ivanov, E. Danshina, Ceram. Int. **44**(18), 22856 (2018).
[24] H. E. Sekrafi, A. B. J. Kharrat, M. A. Wederni, K. Khirouni, N. Chniba-Boudjada, Mater. Res. Bull. **111**, 329 (2019).
[25] S. Roy, C. V Ramana, Org. Chem.**57**, 1029 (2018).
[26] M. Coskun, E. Polat, F. M. Coskun, Z. Durmus, M. Caglar, A. Turut, J. Alloys Compd. **740**, 1012 (2018)
[27] S. Kumar, D. Singh, S. Sandhu, R. Thangaraj, AIP Conf. Proc. **1665**(1), 080021 (2015)
[28] L. Vázquez-Gómez, L. Horvath, E. Kristof, A. De Battisti, Thin Solid Films **515**(4), 1819 (2006)
[29] S. Kumar, D. Singh, R. Thangaraj, Appl. Surf. Sci. **273**, 437 (2013).
[30] A. E. Ozel, D. Deger, S. Celik, S. Yakut, B. Karabak, S. Akyuz, Phys. B Condens. Matter **527**, 72 (2017)
[31] http://materialsproject.org/materials/mp-28230/#
[32] S. Sankar, I Maurya, A. Raj, S. Singh, O. P. Thakur, M. Jayasimhadri, Appl. Phys. A Mater. Sci. Process. **126**(686), 1(2020)
[33] P. Annu, M. Palanisamy, G. Bangaru, S. Ramakrishnan, A. Kandasami, P. Kumar, Appl. Phys. A Mater. Sci. Process. **125**(7), 458 (2019)
[34] H. Baş, N. Kalkan, D. Deger, J. Mater. Sci. Mater. Electron. **27**(7), 7518 (2016).

*Corresponding author: hku@istanbul.edu.tr